Semi-selective image dehazing

Conference Paper · May 2021

CITATIONS
0

READS
43

4 authors, including:

Yin Gao
Chinese Academy of Sciences
27 PUBLICATIONS **45** CITATIONS
SEE PROFILE

Feng Xie
Institut für Automation und Kommunikation
11 PUBLICATIONS **4** CITATIONS
SEE PROFILE

Jun Li
Chinese Academy of Sciences
48 PUBLICATIONS **92** CITATIONS
SEE PROFILE

Semi-selective image dehazing

Yin Gao [1], Huiqin Xu [1,2], Feng Xie [3], Jun Li [1*]

1. Quanzhou Institute of Equipment Manufacturing, CAS, Quanzhou, 362200
E-mail: yngaoyin@163.com

2. Lanzhou Jiaotong University, Lanzhou, 730070, China
E-mail: 15821985817@163.com

3. Institute of Automation and Communication, 39106, Magdeburg, Germany
E-mail: Feng.Xie@ifak.eu

Abstract: In this paper, we propose a new image dehazing method via the semi-selective method. Firstly, we obtain the effect range of the global atmospheric light according to the statistical prior method. Secondly, a relative total variation with adaptive boundary constraint is developed to optimize the transmission. Finally, a semi-selective method is used to select the image with the best visual sense. Experimental results show that our method outperforms state-of-the-art haze removal methods in dehazing visual effects.

Key Words: image dehazing; adaptive boundary constraint; semi-selective

1 Introduction

As we all know, Hazy weather interferes with unmanned driving, satellite observation and outdoor mobile smart devices to obtain targets, which will cause misjudgments and have a greater impact on the safety of traveling[1], [2]. Therefore, image dehazing has been researched by more and more scholars.

In recent years, several methods have been developed for image dehazing, and have achieved varying degrees of success, which can be roughly divided into three categories: enhancement-based algorithms, prior-based algorithms, and learning-based algorithms.

Image enhancement methods focus on improving the contrast of haze images and highlighting image details. Such as histogram equalization[3], wavelet transform[4], and Retinex[5]. Representative work includes Retinex [5], [6], [7], [8]. Wang et al.[6]propose a dehazing model by using multi-scale Retinex to compute the atmospheric light value and transmission map. Liu et al.[7]notice the relationship between image dehazing and Retinex, then formulate the dehazing problem as the minimization of a variational Retinex model. Tang et al.[8] propose an approach using Retinex and dark channel prior for nighttime image dehazing. However, enhancement based image restoration methods usually cause unfavorable visual effects such as over-enhancement or loss of information.

To solve these problems, the atmospheric scattering model [9]is proposed and developed a series of prior based methods [10], [11], [12], [13], [14]. Fattal[10]presents a refined image formation model that accounts for surface shading and scene transmission. Tarel et al.[11]propose an approach for visibility restoration based on median filtering. Zhu et al.[12]use a linear model for the scene depth of the haze image based on the color attenuation prior. Biu et al.[13]estimate the transmission values by constructing a statistical color ellipsoid. Among them, the major advancement is the proposal of the dark channel prior method (DCP) by He et al.[14]. However, the DCP method is not real-time and it causes color distortion for large bright white areas. After that, many methods are based on this theory, such as [15], [16], [17], [18], [19], [20], [21]. Wang et al.[16]estimate the transmission of the sky and non-sky regions separately, then combine them to dehaze. Li et al.[17] decompose the glow image from the nighttime haze image, then estimate transmission by using DCP. Zhang et al.[18]extract bright white objects in haze image by saliency detection, then using dark channel image to estimate the coefficients in the atmospheric model. Yang et al.[19]present a tolerance mechanism that determines the tolerance value adaptively according to the image characteristics.

Recently, several state-of-the-art learning-based methods have been introduced to directly calculate the transmission and atmospheric light[22], [23], [24], [25]. Cai et al.[22]propose the DehazeNet deep architecture, which uses CNNs to embody existing image dehazing priors. Yeh et al.[23]propose an architecture called MSRL-DehazeNet according to image decomposition framework and multi-scale residual CNN. Park et al.[24]present a system to combine two heterogeneous GAN models. In this framework, CycleGAN generates haze-free images, and cGAN preserves textual details. Li et al.[25]present a zero-shot dehazing method, which is an unsupervised learning algorithm that doesn't use any haze-free images. Meanwhile, many end-to-end dehazing trainable architectures have been proposed[26], [27], [28], which don't estimate the transmission and atmospheric light, but directly output haze-free images. Liu et al.[26]uses three modules to build a network named Grid DehazeNet. Although learning-based approaches have shown significant influence for haze removal, most existing methods in a supervised manner that uses synthetic images to train.

To address these problems, we propose a semi-selective method for haze removal. Specifically, to reduce halo artifacts and improve the visual quality, we segment the sky region relying on Gaussian filtering, histogram statistics, and dichotomy to calculate the range of atmospheric light

*This work is supported by the Scientific and Technological Project of Quanzhou (No.2019C009R).

values. Then, we optimize the transmission by using a relative total variation in each global atmospheric light. Finally, we choose the maximum visual value to find the best result among the initial restoration images. With the semi-selective approach, our model performs better than the state-of-the-art haze removal methods.

The main contributions of our method are as follows:

- A statistical prior is developed to obtain the range of atmospheric light.
- In each atmospheric light, the transmission is optimized by a relative total variation with adaptive boundary constraint.
- A semi-selective method is proposed to obtain the best visual image.

2 Proposed method

The proposed image dehazing based on the semi-selective method will be presented in this section. First, the effect range of the global atmospheric light is obtained according to the statistical prior method. Subsequently, the transmission is optimized by a relative total variation with adaptive boundary constraint. Based on the DCP model, several initial dehazing images are obtained. Finally, a semi-selective method is used to select the image with the best visual sense.

The classic DCP model [29] comes from the atmospheric scattering model, and usually can be described as follows.

$$I(x)=J(x)t(x)+A(1-t(x)), \tag{1}$$

where $I(x)$ is an input hazy image. $J(x)$ is a hazy-free image. $t(x)$ is the transmission. A represents the global atmospheric light.

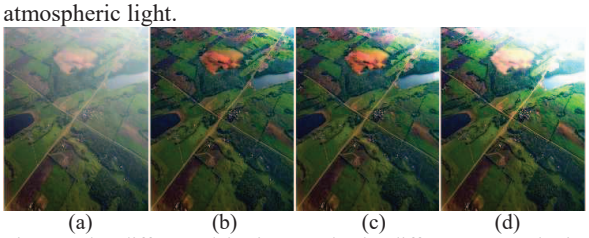

(a) (b) (c) (d)

Fig. 1. The different dehazing results in different atmospheric background light values. (a) The hazy image. (b) The dehazing image A=229. (c) The dehazing image A=203. (d) The dehazing image A=150.

2.1 Estimating the range of atmospheric light

In dehazing analysis, we find that the atmospheric light affects the brightness of the dehazing image. When the brightness of the input image is excessive, the halo phenomenon will appear in the dehazing. Therefore, it is important to effectively estimate the range of global atmospheric light for improving the visual effects of fog image restoration. Fig. 1 gives an example of the different dehazing results in different atmospheric background light values. As the atmospheric light value decreases, the dehazing image becomes brighter, and the details in the image are gradually lost. Therefore, we need to specify a range of effective atmospheric light values to reduce the amount of calculation and improve the quality of dehazing.

To solve these problems, we adopt a statistical prior method to segment the sky region. Firstly, the input hazy image is smoothed by the Gauss filtering. Secondly, the histogram statistics are performed on each channel image. Finally, the location of the penultimate trough is obtained using the dichotomy, which is the threshold point for dividing the sky region. The solution is as follows.

$$\begin{cases} G(x)=f_g(I(x)) \\ a_c=\underset{x\in[0,255]}{\operatorname{argmax}}\left(x \mid G_c'(x)=0, G_c''>0\right), c\in\{r,g,b\} \end{cases}, \tag{2}$$

where a_c is a threshold for segmenting sky regions in each channel of a hazy image. f_g is a Gaussian filter. $G(x)$ is the filtered result by f_g. $G_c'(x)$ denotes the first derivative. G_c'' denotes the second derivative.

To estimate the range of the global atmospheric light A more effectively, we reformulate A by.

$$A=[\min(a_c), mean(a_c), \max(a_c)], \tag{3}$$

To illustrate the robustness of our segmentation algorithm, we randomly selected six hazy images for segmentation experiments, as shown in Figure 2. Fig.2(a,c,e) shows the hazy images. Fig.2(b,d,f) shows the segmentation results of these corresponding hazy images.

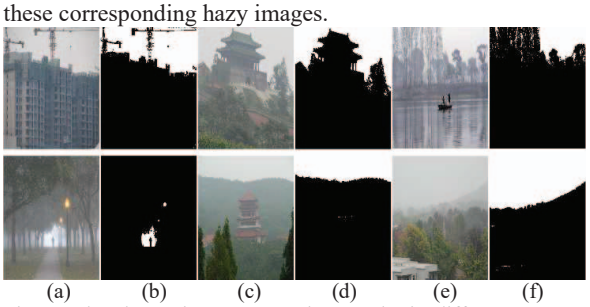

(a) (b) (c) (d) (e) (f)

Fig. 2. The sky region segmentation results in different scenes. (a,c,e) The hazy images. (b,d,f) the corresponding segmented images of gray images.

2.2 Optimizing the transmission

In the DCP, the dark channel image is obtained by the minimum filtering method, but this method will cause a serious loss of brightness of the processed image. For the optimization of transmission, if the optimizing method is not appropriate, it will cause a certain halo phenomenon. Therefore, a relative total variation with adaptive boundary constraint is proposed to solve the problem.

Firstly, according to the radiance cube definition[15], we define an adaptive boundary constraint of an arbitrary haze image with underneath translation to obtain the dark channel image. The formula is as follows.

$$t_i(x)=\min_{i\in[1,\ldots,k]}\left\{\max_{c\in[r,g,b]}\left(\frac{A_i-I_c(x)}{A_i-C_0^c(x)}, \frac{A_i-I_c(x)}{A_i-C_1^c(x)}\right)\right\}, \tag{4}$$

where $t_i(x)$ is the transmission with the boundary constraint in each global atmospheric light. $C_0^c(x)$ represents the minimum value of color channel pixel, $C_0^c(x)=\min_{c\in[r,g,b]}(I_c(x))$. $C_1^c(x)$ represents the maximum value of color channel pixel, $C_1^c(x)=\min_{c\in[r,g,b]}(I_c(x))$. A_i contains the range of the global atmospheric light by (3). Here, $I_c(x)$ is the reduced image, and the reduction factor is 1/4.

To suppress insignificant abrupt depth jumps and maintain major edges for the transmission, we develop a

relative total variation method. The optimization process is as follows.

$$nt_i(x) = \underset{i\grave{o}[1,\ldots,k]}{f_t}\left(t_i(x)\right), \tag{5}$$

where f_t is the image smoothing method via the relative total variation method[30]. $nt_i(x)$ is the optimized transmission in each global atmospheric light A. Fig.3 shows the transmission optimization process in A_1.

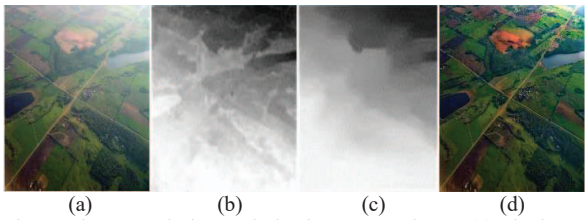

(a) (b) (c) (d)

Fig. 3. The transmission optimization process in A_1. (a) The hazy image. (b) The dark channel image. (c) The optimized transmission. (d) The dehazing image.

2.3 Semi-selective dehazing

After the optimizing transmission, the initial dehazing images are obtained based on different global atmospheric light values and optimized transmission. The initial dehazing results are obtained as follows.

$$J_i(x) = \frac{I(x) - A_i}{\left(\max\left(nt_i(x), t_0\right)\right)^{dt}} + A_i, i\grave{o}\{1,..,k\}, \tag{6}$$

where $J_i(x)$ is an initial dehazing result. dt is an adjustable parameter in the range of [0,1]. t_0 is the lower bound of the transmission $nt_i(x)$.

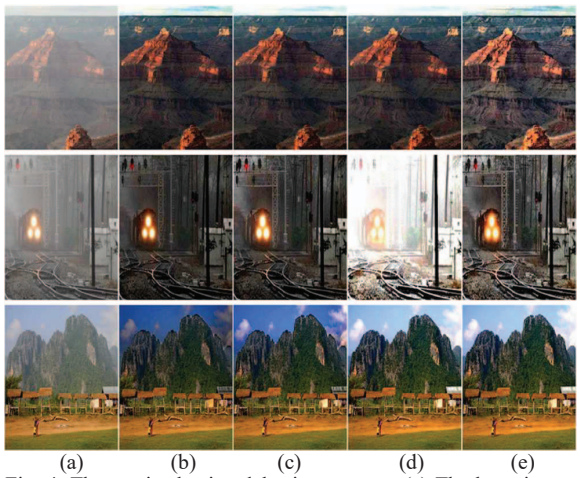

(a) (b) (c) (d) (e)

Fig. 4. The semi-selective dehazing process. (a) The hazy image. (b-d) The initial dehazing image. (e) The final dehazing image.

Due to a large number of initial restoration results, we design a semi-selective method to extract the best visual image. Firstly, the dual vision evaluation method is used to obtain the visual value of the input images. The greater the visual perception value, the better the image quality. Second, the maximum value is obtained by the bubbling method. Finally, the final selective dehazing image is extracted in the place of maximum visual perception. The extraction rules are as follows.

$$Jf(x) = \underset{i\grave{o}[1,\ldots,k]}{FS}\left(J_i(x)\right), \tag{7}$$

where $Jf(x)$ is a final haze-free image. FS denotes a semi-selective method and is computed as.

$$S_i = f_c\left(J_i(x)\right) + f_N\left(J_i(x)\right), \tag{8}$$

where f_c is a function of the contrast-distorted calculation[31]. f_N denotes the perceptual quality of natural image[32]. S_i is the visual value computed by the dual vision evaluation method. $FS = find(x \mid x = \max(S_i))$. After semi-selective dehazing, we use the CLAHE method to adjust the brightness to make the visual effect better.

$$JF(x) = f_{ch}\left(Jf(x)\right), \tag{9}$$

where $JF(x)$ denotes the final dehazing image. f_{ch} is the CLAHE method. Fig. 4 shows the semi-selective dehazing process.

3 Experimental results and analysis

Our method platform in this article is MATLAB on Windows7. To prove the effectiveness of our method, we use subjective and objective evaluation methods. For better comparison, we compare our performance with state-of-the-art methods, such as He et al.[29], Bui et al.[13], Galdran[33], Hu et al.[34], Zhu et al.[35], Dhara et al.[36], respectively.

3.1 Color fidelity analysis

In the classical DCP-based method, color cast is most likely to occur in bright regions of hazy images. Therefore, to better verify the effect of the algorithm on color fidelity, we use hazy images with a large number of bright regions to make this experiment.

Fig. 5 shows the qualitative comparison of color casts. Fig. 5(a) are the hazy images. Fig. 5(b-g) are the results of comparison methods. Fig. 5(h) are the results of our method. Because brightness has a greater impact on the color of an image, we will analyze it from two aspects: image brightness and color cast.

In the aspect of dehazing image brightness, the results of Bui et al. and He et al. have the most serious, followed by Zhu et al. and Dhara et al. The results of Galdran and Hu et al. have no brightness loss. Among them, Hu's method improves the brightness of the dehazing image to a certain extent, but the surface of the dehazing image still has a certain degree of haze. Compared with the results of the six methods, our method can effectively improve the brightness of the dehazing image and enhance the details of the target.

As shown in Fig. 5, all the seven methods can remove the haze but vary in color fidelity. Bui et al., He et al., Zhu et al. and Dhara et al. suffer from serious halo artifacts in the sky regions. Galdran and Hu et al.'s results have no halo artifacts in the sky regions. Nevertheless, Galdran's method appears color cast in the dehazing image, Hu et al.'s results remain a little hazy in Fig. 5(d). Compared with the results of the six methods, our results have achieved the best visual effects. The sky regions keep good color fidelity and the objects in these dehazing images are visible in Fig. 5(h).

3.2 Subjective and objective comparative analysis

To verify the effectiveness of the algorithm, this paper selects three types of hazy images with a relatively large and a small sky area and a centered sky region. Fig. 6 shows the qualitative comparison with the different dehazing methods for natural environment images. Fig. 6(a) shows the hazy images (Mountains, Forest, Hut, Slope, City, Crowd). Fig. 6(b-g) depicts the results of the six comparison methods. Fig. 6(h) is the result of our method.

In Fig. 6, all seven methods can remove the haze for natural environment images, but the visual effect of the dehazing image is different. As shown in Fig. 6(b), the results of He et al. remove most of the haze but significantly suffer from over-enhancement. The sky regions of these images appear halo artifacts. The method has the worst visual performance, followed by Bui et al. In fig6(c), the mountain vegetation appears over-enhanced, and the sky region suffers from the halo problem. The results of Zhu et al. have a similar problem as Dhara et al.'s results in Fig. 6(f) and Fig. 6(g). These two methods also suffer from the over-enhanced problem. These dehazing images appear a slight halo phenomenon in the sky regions, and the brightness of these images is also lost. The results of Galdran and Hu et al. have a better visual effect. Nevertheless, the dense haze in the distance cannot be validly removed by Galdran in Fig. 3(d,e). The method of Hu et al. is the best among these six methods, but the contrast of the dehazing image is slightly excessive for low-brightness images.

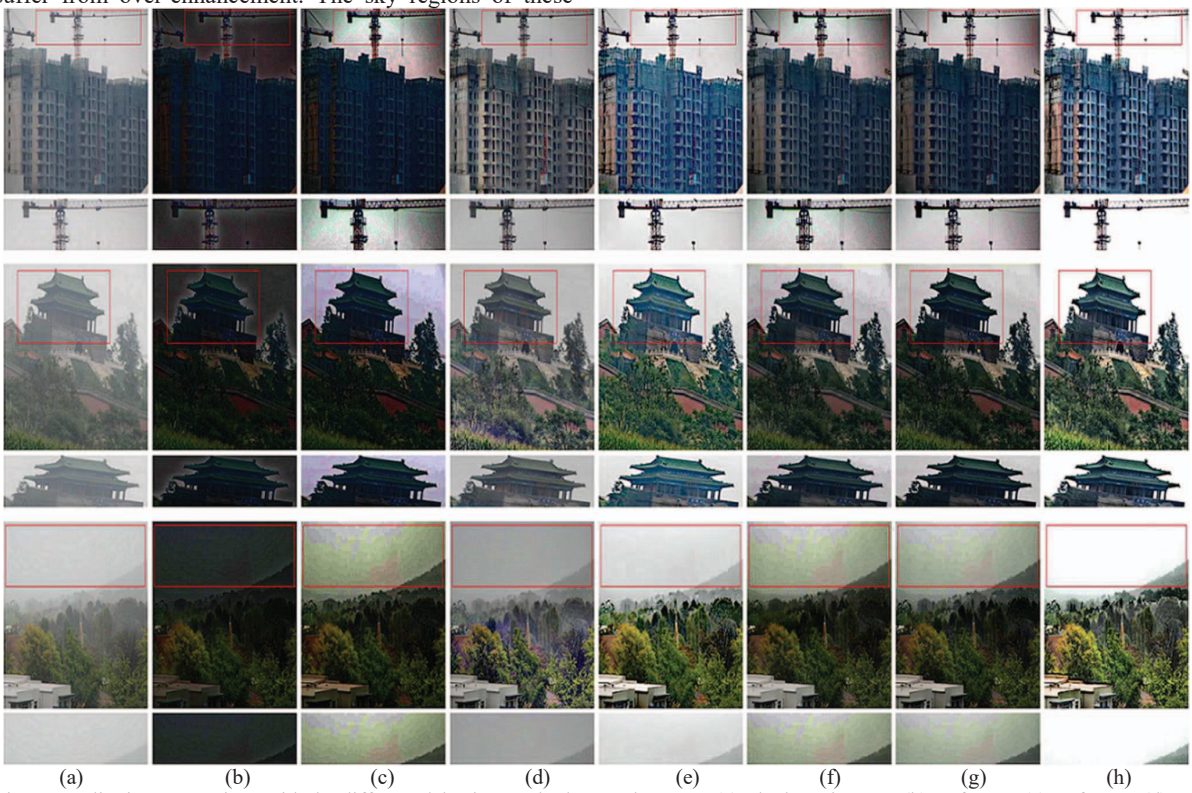

(a) (b) (c) (d) (e) (f) (g) (h)

Fig. 5. Qualitative comparison with the different dehazing methods on color casts. (a) The hazy images. (b) Ref. [29]. (c) Ref. [13]. (d) Ref. [33]. (e) Ref. [34]. (f) Ref. [35]. (g) Ref. [36]. (h) Ours.

Compared with the results of the six methods, our results have achieved the best visual effects. In Fig. 6(h), it can be seen that six images are free from oversaturation. Our method can keep the details of the dehazing images when increasing the brightness of the image. In the figure, the target can be seen far away.

In the objective experiment, we use two indicators: no-reference focus on quality assessment (NR-FQA)[37] and entropy-based no-reference image quality assessment (ENIQA) [38] to evaluate the dehazing results of various methods. A higher ENIQA score indicates a more visual effect of the dehazed image. A lower NR-FQA score implies less blurriness of the input image. The results are list in Table1. Best and second-best results are marked in boldface.

In Tab. 1, for the NR-FQA value, our method produces five sets of minimum values, followed by Hu et al.'s method, which produced three. Bui et al.'s method is weaker than Hu et al.'s method, which produced two sets of minimum values. Dhara et al. is close to Zhu et al., produce one set of minimum values. He et al.'s method is similar to Galdran's method, which has no set of minimum values. For the ENIQA value, our method also has five sets of maximum values. Hu et al.'s method have three sets of maximum values, followed by Bui et al., Galdran and Zhu et al. which have one set of maximum values. Dhara et al. and He et al. have no sets of maximum values. The situation of objective data analysis is consistent with the subjective analysis of dehazing results.

4 Conclusion

In this work, we proposed a Semi-selective image dehazing method. According to the statistical prior method of hazy images, the effective range of global atmospheric light can be estimated by segmenting sky regions. Furthermore, we designed a relative total variation with adaptive boundary constraint to optimize the transmission.

Finally, a semi-selective dehazing method is proposed to select and optimize the dehazing images. Through subjective and objective experimental analysis, our method performs favorably against some state-of-the-art methods on image visibility.

Acknowledgment

This work was supported by the Scientific and Technological Project of Quanzhou (No.2019C009R)

(a) (b) (c) (d) (e) (f) (g) (h)

Fig. 3. Qualitative comparison with the different dehazing methods for natural environment images. (a) The hazy images. (b) Ref. [29]. (c) Ref. [13]. (d) Ref. [33]. (e) Ref. [34]. (f) Ref. [35]. (g) Ref. [36]. (h) Ours

Table1. The objective comparison with the different dehazing methods

	Mountains	Forest	Hut	Slope	City	Crowd
N/E	19.47/**0.26**	-9.09/0	-1.68/0	14.70/0.03	-10.77/0.03	-8.94/0.12
Ref. [29]	7.58/0.22	-8.48/0.18	-4.07/0.14	12.59/0.10	-11.10/0.10	-19.76/0.14
Ref. [13]	6.85/0.22	-26.13/0.16	**-32.59**/0.13	-3.05/0.09	**-27.75/0.21**	-27.07/0.13
Ref. [33]	0.63/0.12	-18.64/0.02	-18.23/**0.36**	3.57/0.10	-16.15/0.14	-18.00/0.14
Ref. [34]	**-21.24**/0.15	-25.47/**0.26**	-27.19/0.34	**-8.59/0.26**	-20.93/0.14	**-30.02/0.21**
Ref. [35]	5.16/0.17	-25.22/0.07	**-31.81**/0.06	8.91/0.02	-22.20/0.13	-25.62/**0.17**
Ref. [36]	4.87/0.17	**-26.25**/0.07	-24.43/0.11	5.71/0.08	-12.28/0.14	-25.75/0.17
our	**-3.16/0.28**	**-28.04/0.39**	-28.04/**0.38**	**-3.83/0.15**	**-28.91/0.15**	**-31.22**/0.14

References

[1] S. G. Narasimhan and S. K. Nayar, Contrast restoration of weather degraded images, *IEEE Trans. Pattern Anal. Mach. Intell.*, 25(6): 713–724, 2003.

[2] A. K. Tripathi and S. Mukhopadhyay, Single image fog removal using anisotropic diffusion, *IET image Process.*, 6(7): 966–975, 2012.

[3] T. K. Kim, J. K. Paik, and B. S. Kang, Contrast enhancement system using spatially adaptive histogram equalization with

temporal filtering, *IEEE Trans. Consum. Electron.*, 44(1): 82–87, 1998.
[4] A. A. Abdelwahab, M. K. Ahmed, and S. H. Hashem, Image enhancement using a contrast measure in the discrete wavelet transform, in *2007 National Radio Science Conference*, 2007: 1–11.
[5] K. R. Joshi and R. S. Kamathe, Quantification of retinex in enhancement of weather degraded images, in *2008 International Conference on Audio, Language and Image Processing*, 2008: 1229–1233.
[6] K. Lu, N. He, J. Xue, L. Shao, and J. Wang, Single Image Dehazing Based on the Physical Model and MSRCR Algorithm, *IEEE Trans. Circuits Syst. Video Technol.*, 28(9): 2190–2199, 2017.
[7] Y. Liu, J. Shang, L. Pan, A. Wang, and M. Wang, A Unified Variational Model for Single Image Dehazing, *IEEE Access*, 7: 15722–15736, 2019.
[8] Q. Tang, J. Yang, X. He, W. Jia, Q. Zhang, and H. Liu, Nighttime image dehazing based on Retinex and dark channel prior using Taylor series expansion, *Comput. Vis. Image Underst.*, 202: 103086, 2020.
[9] A. Cantor, Optics of the atmosphere: scattering by molecules and particles, *IEEE J. Quantum Electron.*, 14(9): 698–699, 1978.
[10] R. Fattal, Single image dehazing, *ACM Trans. Graph.*, 27(3): 1–9, 2008.
[11] J.-P. Tarel and N. Hautiere, Fast visibility restoration from a single color or gray level image, in *2009 IEEE 12th International Conference on Computer Vision*, 2009: 2201–2208.
[12] Q. Zhu, J. Mai, and L. Shao, A fast single image haze removal algorithm using color attenuation prior, *IEEE Trans. Image Process.*, 24(11): 3522–3533, 2015.
[13] T. M. Bui and W. Kim, Single image dehazing using color ellipsoid prior, *IEEE Trans. Image Process.*, 27(2): 999–1009, 2018.
[14] K. He, J. Sun, and X. Tang, Single image haze removal using dark channel prior, *IEEE Trans. Pattern Anal. Mach. Intell.*, 33(12): 2341–2353, 2011.
[15] G. Meng, Y. Wang, J. Duan, S. Xiang, and C. Pan, Efficient image dehazing with boundary constraint and contextual regularization, in *Proceedings of the IEEE International Conference on Computer Vision*, 2013: 617–624.
[16] G. Wang, G. Ren, L. Jiang, and T. Quan, Single image dehazing algorithm based on sky region segmentation, *Inf. Technol. J.*, 12(6): 1168, 2013.
[17] Y. Li, R. T. Tan, and M. S. Brown, Nighttime haze removal with glow and multiple light colors, in *Proceedings of the IEEE International Conference on Computer Vision*, 2015: 226–234.
[18] L. Zhang, S. Wang, and X. Wang, Saliency-based dark channel prior model for single image haze removal, *IET Image Process.*, 12(6): 1049–1055, 2018.
[19] F. Yang and S. Tang, Adaptive Tolerance Dehazing Algorithm Based on Dark Channel Prior, *Algorithms*, 13(2): 45, 2020.
[20] Y. Iwamoto, N. Hashimoto, and Y. W. Chen, Real-Time Haze Removal Using Normalised Pixel-Wise Dark-Channel Prior and Robust Atmospheric-Light Estimation, *Appl. Sci.*, 10(3): 1165, 2020.
[21] J. Jackson, S. Kun, K. O. Agyekum, A. Oluwasanmi, and P. Suwansrikham, A Fast Single-Image Dehazing Algorithm Based on Dark Channel Prior and Rayleigh Scattering, *IEEE Access*, 8: 73330–73339, 2020.
[22] B. Cai, X. Xu, K. Jia, C. Qing, and D. Tao, Dehazenet: an end-to-end system for single image haze removal, *IEEE Trans. Image Process.*, 25(11): 5187–5198, 2016.
[23] C.-H. Yeh, C.-H. Huang, and L.-W. Kang, Multi-scale deep residual learning-based single image haze removal via image decomposition, *IEEE Trans. Image Process.*, 29: 3153–3167, 2019.
[24] J. Park, D. K. Han, and H. Ko, Fusion of Heterogeneous Adversarial Networks for Single Image Dehazing, *IEEE Trans. Image Process.*, 29: 4721–4732, 2020.
[25] B. Li, Y. Gou, J. Z. Liu, H. Zhu, J. T. Zhou, and X. Peng, Zero-shot image dehazing, *IEEE Trans. Image Process.*, 29: 8457–8466, 2020.
[26] X. Liu, Y. Ma, Z. Shi, and J. Chen, Griddehazenet: Attention-based multi-scale network for image dehazing, in *Proceedings of the IEEE International Conference on Computer Vision*, 2019: 7314–7323.
[27] W. Zhang, L. Dong, X. Pan, J. Zhou, L. Qin, and W. Xu, Single Image Defogging Based on Multi-Channel Convolutional MSRCR, *IEEE Access*, 7: 72492–72504, 2019.
[28] W. Ren, L. Ma, J. Zhang *et al.*, Gated fusion network for single image dehazing, in *IEEE Conference on Computer Vision and Pattern Recognition*, 2018: 3253–3261.
[29] K. He, J. Sun, and X. Tang, Single image haze removal using dark channel prior, *IEEE Trans. Pattern Anal. Mach. Intell.*, 33(12): 2341–2353, 2011.
[30] L. Xu, Q. Yan, Y. Xia, and J. Jia, Structure Extraction from Texture via Relative Total Variation, 31(6): 1–10, 2012.
[31] J. Yan, J. Li, and X. Fu, No-reference quality assessment of contrast-distorted images using contrast enhancement, *arXiv Prepr. arXiv1904.08879*, 2019.
[32] K. Gu, J. Zhou, J.-F. Qiao, G. Zhai, W. Lin, and A. C. Bovik, No-reference quality assessment of screen content pictures, *IEEE Trans. Image Process.*, 26(8): 4005–4018, 2017.
[33] A. Galdran, Image dehazing by artificial multiple-exposure image fusion, *Signal Processing*, 149: 135–147, 2018.
[34] H. M. Hu, Q. Guo, J. Zheng, H. Wang, and B. Li, Single image defogging based on illumination decomposition for visual maritime surveillance, *IEEE Trans. Image Process.*, 28(6): 2882–2897, 2019.
[35] M. Zhu, B. He, J. Liu, and J. Yu, Boosting dark channel dehazing via weighted local constant assumption, *Signal Processing*, 171: 107453, 2020.
[36] S. K. Dhara, M. Roy, D. Sen, and P. K. Biswas, Color Cast Dependent Image Dehazing via Adaptive Airlight Refinement and Non-linear Color Balancing, *IEEE Trans. Circuits Syst. Video Technol.*, 1–1, 2020.
[37] M. S. Hosseini and K. N. Plataniotis, Image Sharpness Metric Based on Maxpol Convolution Kernels, in *2018 25th IEEE International Conference on Image Processing (ICIP)*, 2018: 296–300.
[38] X. Chen, Q. Zhang, M. Lin, G. Yang, and C. He, No-Reference color image quality assessment: from entropy to perceptual quality, *arXiv Prepr. arXiv1812.10695*, 1–12, 2018.